MEASUREMENT-INFORMED NONLINEAR MODAL SYNTHESIS OF 65 CLASSICAL GUITARS

Michele Ducceschi, Riccardo Russo, and Craig J. Webb

Department of Industrial Engineering
University of Bologna
Viale Risorgimento 2, Bologna, Italy
michele.ducceschi@unibo.it
riccardo.russo19@unibo.it
craigjonathan.webb@unibo.it

ABSTRACT

When a classical guitar string is plucked, vibration energy flows through the bridge into the body and is radiated as sound. Synthesising this process for a large collection of instruments requires both an efficient nonlinear string model and a robust method for extracting instrument-specific parameters from measurements. This paper addresses both issues. Starting from the publicly available dataset of Mores, which provides impulse-response measurements on 65 classical guitars, modal parameters of the bridge compliance and of the bridge-to-air radiation path are extracted for each instrument. These feed a nonlinear string model in which transverse vibration is governed by a geometrically exact elastic potential coupled at an interior bridge point to the measured body data. The nonlinear potential is quadratised via the Scalar Auxiliary Variable (SAV) method, so that the equations of motion become linear in a scalar variable and a known gradient vector, even at the continuous level. After time discretisation, the coupled system is inverted through two sequential Sherman–Morrison rank-one updates (one for the bridge coupling, one for the SAV nonlinearity), yielding an $\mathcal{O}(N)$ algorithm per time step. Two regularisation techniques prevent long-term drift of the auxiliary variable. The complete pipeline is demonstrated by synthesising plucked tones across all frets and strings for each of the 65 guitars.

1. INTRODUCTION

The sound of a plucked guitar is shaped by three interacting subsystems: a nonlinear string, a resonant body, and the surrounding air. Modal methods have a long history in the synthesis of such coupled systems [1], since they reduce the dynamics to sets of damped oscillators whose frequencies and damping coefficients can be obtained analytically, from numerical pre-computation, or—as in the present work—from measurement. Provided the coupling terms are handled carefully, the resulting schemes are well-suited to recursive time-stepping and can be made very efficient [2].

The treatment of the string nonlinearity is the main difficulty. At moderate plucking amplitudes, salient perceptual effects come into play, such as pitch glide and spectral enrichment [3, 4]. The underlying potential may be written in geometrically exact form [5] or simplified to the cubic [6, 7] or Kirchhoff–Carrier [6, 8] models. In all cases, except for the Kirchhoff–Carrier model, energy-stable numerical integration has traditionally required linearly or fully implicit solvers. The Scalar Auxiliary Variable (SAV) approach [9], recently applied to string vibration [10, 6, 11, 7, 12] and to modal networks [13], offers a way out: the nonlinear potential is replaced by its square root, introducing a single scalar unknown that renders the equations linear in the unknowns. When this reformulation is combined with the Sherman–Morrison formula [14], the system can be inverted explicitly at $\mathcal{O}(N)$ cost per time step—comparable to a purely linear scheme. Despite this efficiency gain, SAV is prone to numerical pollution observed across various contexts [15, 6, 11, 16]; this has motivated the development of regularisation techniques. Two main regularisation strategies have emerged. The first avoids sign-flipping of the auxiliary variable by imposing a constraint on the gradient of the nonlinear potential [17, 6, 11], while the second adds a servo-correction to prevent long-term drift [18].

Mores [19, 20] has made publicly available the impulse-response measurements of 65 classical and flamenco guitars spanning two centuries of lutherie, from early romantic instruments by Pages and Munoa to modern concert guitars by Bellido and DeVoe. The measurements were carried out at museums, luthier workshops, and private collections across Spain and Germany. Several of the instruments—particularly the Torres and Pages originals held in Barcelona—are tuned to historical pitch and are rarely, if ever, played; others, among the early romantics in the Romanillos collection, lack strings entirely or show significant structural deterioration. For such instruments, the measured impulse response may be one of the last reliable records of their vibro-acoustic behaviour. Coupling this data with a physically faithful synthesis model amounts to preserving the sound of the instrument itself—a principle that lies at the heart of the NEMUS project [21], which aims to build playable numerical replicas of historical instruments held in museum collections. The pipeline developed here can be seen as a concrete, large-scale application of that idea.

This paper describes the complete chain, from raw impulse responses to synthesised audio, and applies it to all 65 guitars in the Mores collection. The string model employs a geometrically exact transverse potential without longitudinal degrees of freedom, reformulated via SAV quadratisation already at the continuous level, utilising both regularisation techniques combined. A signal-processing chain extracts bridge compliance and radiation transfer-function modal parameters from the measured data. In the discrete-time scheme, exact modal parameters eliminate numerical dispersion, a servo correction prevents long-term drift of the auxiliary variable, a constraint avoids sign-flipping, and, extending the single-rank-one SAV schemes of the authors' prior work [6, 7], two sequential Sherman–Morrison steps yield the explicit update for the fully coupled string–bridge system. The result is a library of over 6000 plucked-string samples exhibiting instrument-specific body resonances.

Section 2 presents the continuous-time model and SAV reformulation, with the overall signal path summarised in Fig. 1. Section 3 describes the dataset and the extraction procedure (Fig. 6). Section 4 details the time-stepping scheme. Section 5 reports results, and Section 6 offers concluding remarks.

2. PHYSICAL MODEL

2.1. Nonlinear String

Consider a stiff string of length L, linear density μ (kg/m), pretension T_0 (N), cross-sectional area A, Young's modulus E, and second moment of area I. The transverse displacement $u(x, t)$, $x \in [0, L]$, $t \geq 0$, satisfies the partial differential equation (PDE):

$$\mu\, \partial_t^2 u = \mathcal{L}u + \mathcal{F} + \delta_e f_e + \delta_b F_b, \tag{1}$$

with:

$$\mathcal{L} = T_0 \partial_x^2 - EI \partial_x^4 - \mu\sigma\, \partial_t \tag{2}$$

where, ∂_x^j and ∂_t^j represent the j-th partial derivative with respect of x and t respectively, and σ is a constant regulating damping. Note, however, that a "per-mode" damping coefficient will be set directly in the modal domain. The model includes a stiffness term, derived from the Euler-Bernoulli beam theory [22], written in terms of Young's modulus E and the moment of inertia I. f_e and F_b represent, respectively, external pluck forcing and the bridge force reaction. Both are directed pointwise onto the string, with two Dirac's deltas δ_e and δ_b centred on locations x_e and x_b, respectively. $\mathcal{F} = \mathcal{F}(\zeta)$ is a conservative nonlinear force density which depends on the slope $\zeta \triangleq \partial_x u$. The string is assumed simply supported at both ends, and thus: simply-supported boundary conditions:

$$u = \partial_x^2 u = 0, \quad x \in \{0, L\}. \tag{3}$$

2.1.1. *Potential energy and splitting*

It is convenient to split the total potential energy as $V = Q + \phi_{\mathrm{nl}}$, separating the familiar quadratic contributions due to tension and bending,

$$Q(u) = \frac{T_0}{2} \int_0^L (\partial_x u)^2\, \mathrm{d}x + \frac{EI}{2} \int_0^L (\partial_x^2 u)^2\, \mathrm{d}x \geq 0, \tag{4}$$

from a nonlinear residual $\phi_{\mathrm{nl}} \geq 0$. The latter arises from a geometrically exact model in which longitudinal displacements are neglected: a common and useful simplification for the transverse-only case [8]. For a string element with slope ζ, the Green–Lagrange strain reads $\varepsilon = \sqrt{1 + (\zeta)^2} - 1$, and the corresponding elastic energy density is:

$$\mathcal{V}(\zeta) = \frac{G}{2}\big(\sqrt{1+\zeta^2} - 1\big)^2, \tag{5}$$

where $G \triangleq EA - T_0 > 0$ is the nonlinear stiffness parameter. The total nonlinear potential follows by integration:

$$\phi_{\mathrm{nl}}(u) = \int_0^L \mathcal{V}(\partial_x u)\, \mathrm{d}x \geq 0. \tag{6}$$

Non-negativity is immediate since $G > 0$ in musical strings, and the integrand is a perfect square. It is worth noting that this is *not* the Kirchhoff–Carrier model, which replaces the local slope dependence by a spatially averaged strain $\bar{\varepsilon} \propto \int_0^L (\zeta)^2\, \mathrm{d}x$, yielding a simpler rank-one modal coupling. The potential (6) retains the full pointwise dependence on the slope, producing richer nonlinear interactions—spectral enrichment and pitch glide—at large amplitudes [4].

2.1.2. *SAV quadratisation*

The central idea behind the SAV approach [9, 10] is to replace the nonlinear potential by a new scalar unknown whose square tracks the potential energy, thereby rendering the equations of motion linear in the unknowns at each time step. Because the potential ϕ_{nl} is non-negative, one may define the auxiliary variable

$$\psi \triangleq \sqrt{2\phi_{\mathrm{nl}} + \varepsilon}, \tag{7}$$

with $\varepsilon > 0$ a small regularisation constant ensuring that the denominator in the subsequent gradient expression never vanishes. By the chain rule,

$$\dot{\psi} = \left\langle \frac{\delta\psi}{\delta u},\ \partial_t u \right\rangle, \tag{8}$$

where $\langle \cdot, \cdot \rangle$ denotes the L^2 inner product over $[0, L]$. Defining the normalised gradient field

$$g(x) \triangleq \frac{\delta\psi}{\delta u} = \frac{1}{\psi} \frac{\delta\phi_{\mathrm{nl}}}{\delta u}, \tag{9}$$

one recovers $\delta\phi_{\mathrm{nl}}/\delta u = \psi\, g$, and the evolution of ψ takes the compact form

$$\dot{\psi} = \langle g,\ \dot{u} \rangle. \tag{10}$$

The variational derivative of (6) gives $\delta\phi_{\mathrm{nl}}/\delta u = -\partial_x[\mathcal{S}(\zeta)\, \zeta]$, where the stress function reads:

$$\mathcal{S}(\zeta) = G\, \frac{\sqrt{1 + (\zeta)^2} - 1}{\sqrt{1 + (\zeta)^2}}\,. \tag{11}$$

Using these definitions, the equation of motion for the damped, forced, bridge-coupled string takes the SAV-reformulated form:

$$\mu\, \partial_t^2 u = \mathcal{L}u - \psi\, g + \delta_e f_e + \delta_b F_b, \tag{12a}$$

$$\dot{\psi} = \langle g,\ \dot{u} \rangle. \tag{12b}$$

Crucially, this system is *exactly* equivalent to the original PDE (1). The nonlinear force $\mathcal{F}$, however, now appears as the product $\psi\, g$. This factorisation is what will ultimately permit a fully explicit time-stepping scheme.

Left-multiplying (12a) by $\dot{u}$ and integrating over the domain yields the energy balance

$$\frac{d}{dt}\Big(\underbrace{\frac{\mu}{2}\|\dot{u}\|^2}_{K} + Q + \frac{\psi^2}{2} \Big) = -\mu\sigma\|\dot{u}\|^2 + \mathcal{P}, \tag{13}$$

where $\mathcal{P}$ collects the injected power from excitation and bridge coupling. The Hamiltonian $\mathfrak{H} = K + Q + \psi^2/2$ is manifestly non-negative, so that unforced solutions remain bounded for all time.

2.2. Bridge Coupling

The string is attached to a bridge at the interior point $x_b = \xi_b L$ ($\xi_b < 1$; here $\xi_b = 0.995$), through which it drives a compliant body. In the frequency domain, the driving-point compliance of the guitar body is represented by a sum of J modal contributions:

$$H_b(\omega) = \sum_{j=1}^{J} \frac{\beta_j}{\left(\omega_j^b\right)^2 - \omega^2 + 2i\sigma_j^b \omega}, \tag{14}$$

with natural frequencies ω_j^b, damping coefficients σ_j^b, and compliance residues β_j, all obtained from measurement (Section 3). In the time domain, each bridge mode obeys:

$$m_j^b \left(\ddot{r}_j + 2\sigma_j^b \dot{r}_j + \left(\omega_j^b\right)^2 r_j \right) = -\beta_j F_b,\ j=1,\dots,J, \tag{15}$$

where m_j^b are the modal masses, and the total bridge displacement is $u_b = \sum_j r_j$. The string and body are coupled by enforcing displacement compatibility:

$$u(x_b, t) = u_b(t), \tag{16}$$

with the reaction force F_b determined implicitly to satisfy this constraint at every time step.

2.3. Modal Projection and SAV

Under the simply-supported conditions (3), the displacement is expanded over the sinusoidal basis

$$u(x,t) = \boldsymbol{\chi}^{\mathsf{T}}(x)\, \mathbf{q}(t), \quad \chi_m = \sqrt{2/L}\, \sin(m\pi x/L), \tag{17}$$

$m = 1, \dots, M$, where each mode has natural frequency:

$$\omega_m^s = \sqrt{\frac{T_0}{\mu}\Big(\frac{m\pi}{L}\Big)^2 + \frac{EI}{\mu}\Big(\frac{m\pi}{L}\Big)^4}. \tag{18}$$

To improve the system's efficiency, all modes need to participate in the nonlinear interaction. The nonlinear coupling is restricted to modes below a cap $f_{\mathrm{nl}}^{\max}$, i.e. $M_{\mathrm{nl}} = \max\{m : \omega_m/(2\pi) \le f_{\mathrm{nl}}^{\max}\}$; higher modes are computed as linear oscillators. For E2 (≈ 82 Hz), $f_{\mathrm{nl}}^{\max} = 5000$ Hz retains $M_{\mathrm{nl}} \approx 60$ out of $M \approx 200$, yielding a substantial saving with no audible degradation, as verified informally by A/B listening across a range of M_{nl} settings. The evaluation of ϕ_{nl} and of the SAV gradient field g requires knowledge of the slope $\zeta(x,t)$ at a set of spatial grid points. A uniform grid $\{x_i\}_{i=1}^{N_g},\ N_g \in \mathbb{N}$ with spacing $h = L/N_g$ is therefore introduced, and the $N_g \times M_{\mathrm{nl}}$ *differentiated mode matrix* sampled at sample points x_i. $\mathbf{R}$ is defined through:

$$R_{im} = \partial_x \chi_m(x_i) = \sqrt{\frac{2}{L}}\, \frac{m\pi}{L} \cos\Big(\frac{m\pi x_i}{L}\Big), \tag{19}$$

for $m = 1, \dots, M_{\mathrm{nl}}$. The discrete slope vector is then $\boldsymbol{\zeta} = \mathbf{R}\, \mathbf{q}_{\mathrm{nl}}$, with $\mathbf{q}_{\mathrm{nl}} = [q_1, \dots, q_{M_{\mathrm{nl}}}]$, and the potential is evaluated by the trapezoidal quadrature $\phi_{\mathrm{nl}} \approx h \sum_i \mathcal{V}(\zeta_i)$. The SAV gradient is projected back to modal coordinates via

$$\boldsymbol{\eta} = \mathbf{R}^{\mathsf{T}} \mathbf{g}. \tag{20}$$

Note that the computation of the nonlinear gradient value is detailed in the dedicated section 4.3

Concatenating the M string modes $\mathbf{q}$ with the J bridge modes $\mathbf{r}$ into a single state vector $\mathbf{y} = [\mathbf{q};\ \mathbf{r}]$ of length $N \triangleq M + J$, the SAV-reformulated equations of motion for the complete system read:

$$\ddot{\mathbf{y}} + \mathbf{C}\,\dot{\mathbf{y}} + \boldsymbol{\Omega}^2 \mathbf{y} = -\frac{\psi}{\mu}\,\tilde{\boldsymbol{\eta}} + \mathbf{s}\, f_e + \mathbf{f}\, F_b, \tag{21a}$$

$$\dot{\psi} = \boldsymbol{\eta}^{\mathsf{T}} \dot{\mathbf{q}}_{\mathrm{nl}}, \tag{21b}$$

Here, $\tilde{\boldsymbol{\eta}} \triangleq [\boldsymbol{\eta};\ \mathbf{0}_J]$ is a vector embedding $\boldsymbol{\eta}$ into $\mathbb{R}^N$; $\boldsymbol{\Omega}$ and $\mathbf{C}$ are block-diagonal matrices collecting the (squared) natural frequencies and damping coefficients of the string and bridge modes; $\mathbf{s} = [\boldsymbol{\chi}(x_e); \mathbf{0}_J]$ distributes the pluck force; and $\mathbf{f}$ distributes the bridge reaction:

$$\mathbf{f} = \big[\boldsymbol{\chi}(x_b)/\mu;\ -\boldsymbol{\beta} \oslash \mathbf{m}^b\big], \tag{22}$$

with $\boldsymbol{\beta} = [\beta_1, \dots, \beta_J]^{\mathsf{T}}$, and $\mathbf{m}^b = [m_1^b, \dots, m_J^b]^{\mathsf{T}}$. The symbol $\oslash$ indicates element-wise division, and ";" is intended for column-wise vector concatenation. The reaction force is obtained by left-multiplying (21a) by

$$\mathbf{v}^{\mathsf{T}} \triangleq \big[\boldsymbol{\chi}_b; -\boldsymbol{\beta}\big]^{\mathsf{T}} \boldsymbol{\Omega}^{-2}. \tag{23}$$

and solving for F_b. Taking into account the compatibility constraint (16), which may be rewritten $\big[\boldsymbol{\chi}_b; -\boldsymbol{\beta}\big]^{\mathsf{T}} \mathbf{y} = 0$, Eq. (21a) becomes:

$$\mathbf{T} \left(\ddot{\mathbf{y}} + \mathbf{C}\,\dot{\mathbf{y}} + \frac{\psi}{\mu} \tilde{\boldsymbol{\eta}} - \mathbf{s}\, f_e \right) = -\boldsymbol{\Omega}^2 \mathbf{y}, \tag{24}$$

with F_b now embedded into the matrix $\mathbf{T} \triangleq \mathbf{I} - \mathbf{f}(\mathbf{v}^{\mathsf{T}}\mathbf{f})^{-1}\mathbf{v}^{\mathsf{T}}$.

String losses follow the two-parameter model of Woodhouse [23], which expresses the modal damping coefficient as a linear function of angular frequency:

$$c_m = \sigma_{0,s} + \frac{\eta_{f,s}}{2}\, \omega_m, \qquad \sigma_{0,s} = \frac{6 \ln 10}{T_{60,s}}, \tag{25}$$

where $T_{60,s}$ is the T_{60} at the fundamental of string s and $\eta_{f,s}$ (units: s) is the per-string viscous-loss coefficient measured by Woodhouse [23] for D'Addario Pro Arte hard-tension strings.

The total energy of the coupled modal system,

$$\mathfrak{H} = \frac{1}{2}\dot{\mathbf{y}}^{\mathsf{T}}\dot{\mathbf{y}} + \frac{1}{2}\mathbf{y}^{\mathsf{T}}\boldsymbol{\Omega}^2\mathbf{y} + \frac{\psi^2}{2} \ge 0, \tag{26}$$

is non-negative, ensuring numerical stability in the unforced case.

2.4. Radiation

Once the bridge force is known, it drives the bridge-to-air radiation transfer, modelled here as a modal reverberator whose frequency response takes the pole-residue form:

$$H_{\mathrm{rad}}(\omega) = \sum_{l=1}^{N_r} \frac{b_l}{i\omega - p_l} + \frac{\bar{b}_l}{i\omega - \bar{p}_l}, \tag{27}$$

with poles $p_l = -\sigma_l^r + i\omega_l^r$ and real residues b_l, extracted separately for the bass and treble sides of the bridge. Each complex-conjugate pole pair is realised in the time domain as a parallel second-order IIR section [24]. A stereo output is obtained via mid-side width processing of the two resulting signals.

2.5. Excitation

The pluck force $f_e(t)$ is derived from a recorded impulse, resampled to the synthesis rate, normalised, and scaled by a peak amplitude $F_{\max}$. To introduce natural timbral variation across notes—mimicking the small positional inconsistencies of a real player—the pluck position $\xi_e = x_e/L$ is randomised within $[\xi_e^{\min}, \xi_e^{\max}]$ for each note.

3. THE MORES DATASET AND PARAMETER EXTRACTION

3.1. The Guitar Collection

The Mores archive [19, 20] documents 65 guitars whose construction dates span from 1803 to 2018. The collection includes *early romantic* instruments by Pages, Munoa, and Martinez; four *Torres* originals (1859–1889, one with a papier-mâché back); *classical Spanish* concert guitars by Fleta, Garcia, Contreras, Bellido, and Ramirez; and *flamenco* blancas and negras by Conde, Reyes, and DeVoe, among others. Scale lengths range from 551 to 668 mm and total weights from 670 g to over 1750 g.

The instruments were measured across seven sites in Spain and Germany between September 2018 and March 2019, including luthier studios in Granada, the Centro de Documentación Musical de Andalucía, the Museu de la Música in Barcelona, the anechoic facility at the Hamburg University of Applied Sciences, and the private collection of José Romanillos. Several museum pieces—notably the Torres and Pages originals in Barcelona—are tuned to historical pitch (415 or 392 Hz) and are never played in concert; others among the Romanillos early romantics lack strings entirely or exhibit structural damage. The synthesis pipeline developed here gives these silent instruments a voice.

3.2. Measurement Setup

Each guitar was excited at the bridge saddle with a miniature impulse hammer (Dytran 5800SL, 9.8 g). The response was captured by two wax-mounted accelerometers (Kistler 8778A500, 0.4 g each) on the treble and bass sides of the bridge, and by three $\frac{1}{4}''$ IEPE microphones (ROGA MI-17) positioned 10 cm above the top plate; all channels were digitised at 48 kHz / 24-bit. The guitar rested on the lower block and neck only, leaving the body free to vibrate, and a portable floor absorber suppressed reflections at each site. Three to twelve strikes were recorded per impact position; a single best impulse per position was retained based on a 10 N force threshold and -30 dB double-hit rejection. The qualified responses, truncated to one second, form the input to the extraction pipeline. Only the treble-side pairs are used here. The measurement setup is depicted in Fig 3

3.3. Frequency Response Functions

The raw time-domain signals are converted to physical SI units using the manufacturer-supplied sensitivities. The frequency response function is estimated via the H_1 estimator:

$$H(\omega) = \frac{Y(\omega)\overline{F(\omega)}}{|F(\omega)|^2}, \tag{28}$$

and the corresponding impulse response is recovered by inverse DFT.

3.4. Bridge Compliance Extraction

The bridge accelerance $H_{\mathrm{acc}}(\omega)$ is obtained from the hammer–accelerometer channel. Following prior work on modal parameter extraction for reverberation from measured responses [25], the extraction proceeds as follows:

1. **Windowing.** The impulse response is truncated to N_{keep} samples (3000 at 48 kHz) and tapered with a raised-cosine fade-out, reducing spectral leakage while preserving early modal content.
2. **Peak picking.** Local maxima of $|H_{\mathrm{acc}}|$ (in dB) are identified over $[20, 10000]$ Hz, subject to a minimum prominence of 0.5 dB and a minimum spacing of 1 Hz; weak peaks are discarded by an amplitude cap.
3. **Damping estimation.** For each retained peak, the -3 dB bandwidth is measured by interpolation in a $\pm 15\%$ frequency window, yielding $\sigma_j = \Delta\omega_{-3\,\mathrm{dB}}/2$.
4. **Residue fitting.** A modal basis for the accelerance is constructed:
$$[\Psi]_j = \frac{\beta_j^{acc}}{\left(\omega_j^b\right)^2 - \omega^2 + 2i\sigma_j\omega}, \tag{29}$$
The accelerance residues β_j^{acc} are then determined by Tikhonov-regularised least squares, constrained to be real.
5. **Compliance conversion.** The compliance residues are obtained as $\beta_j = \beta_j^{\mathrm{acc}}/(-\omega_j^2)$, and (14) is therefore obtained by summing all contributions for $j = 1, \ldots J$.
6. **Physical filtering.** Modes satisfying $\omega_j < 0.2\sigma_j$ are discarded as overdamped.

Figure 4 shows the results of the accelerance parameters extraction for guitar no. 55, illustrated in Fig. 2.

3.5. Radiation Transfer Function Extraction

The radiation FRF (pressure per unit force), obtained from the hammer–microphone channel, is extracted by an analogous procedure. The modal basis now takes the pole-residue form $[\Phi]_{kl} = (i\omega_k - p_l)^{-1} + (i\omega_k - \bar{p}_l)^{-1}$, with $p_l = -\sigma_l + i\omega_l^d$ and pole damping estimated from the measured -3 dB half-bandwidth. Two separate fits—one for the bass side and one for the treble side of the bridge—produce the radiation filter pair that will later generate the stereo output. Figure 5 shows the results of the radiation modal parameter extraction for the bridge of guitar no. 55.

4. DISCRETE-TIME SYNTHESIS

The continuous-time system (21) is now discretised in time. Two features of the resulting scheme are worth highlighting at the outset. First, the modal frequencies and damping coefficients are corrected so that each *uncoupled* mode reproduces its analytic solution exactly—eliminating numerical dispersion, which would otherwise detune the partials. Second, the coupling terms (bridge and SAV nonlinearity) each contribute a rank-one modification to a diagonal system matrix, so that the entire update can be carried out via two sequential applications of the Sherman–Morrison formula at $\mathcal{O}(N)$ cost.

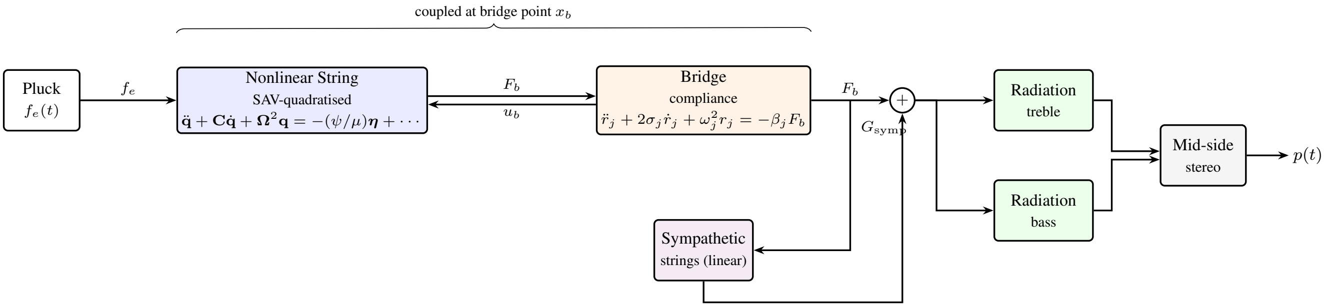

Figure 1: Block diagram of the guitar synthesis model. The SAV-quadratised nonlinear string and bridge compliance are coupled bidirectionally at x_b; F_b drives radiation filters and the sympathetic string bank.

Figure 2: Top view of guitar no. 55, a *Manuel Munoa* from 1803. Adapted from Mores [19].

Figure 3: Mores' Measurement setup. The guitar being measured is no. 23, an *Arangel Fernandez* from 1981. Adapted from Mores [19].

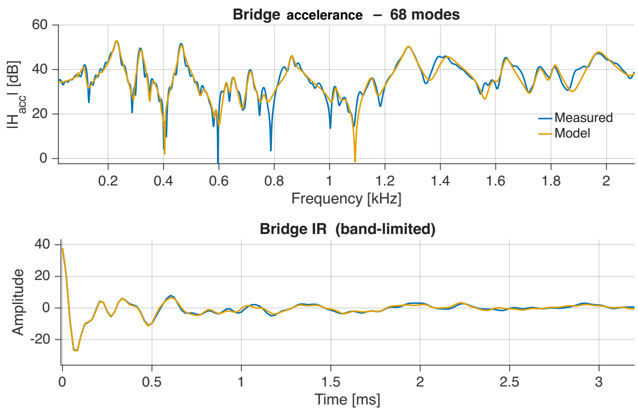

Figure 4: Results of the bridge compliance parameters extraction for guitar no. 55. Top: bridge accelerance. Bottom: time-domain impulse response. The blue line indicates the measured signal and the yellow line the reconstructed one. Plots are zoomed in for clarity.

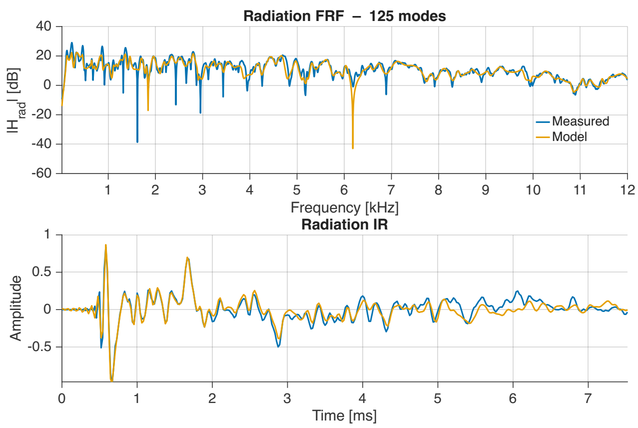

Figure 5: Results of the radiation modal parameter extraction for the bridge of guitar no. 55. Top: Frequency Response Function (FRF). Bottom: time domain impulse response. Color coding as in Fig. 4.

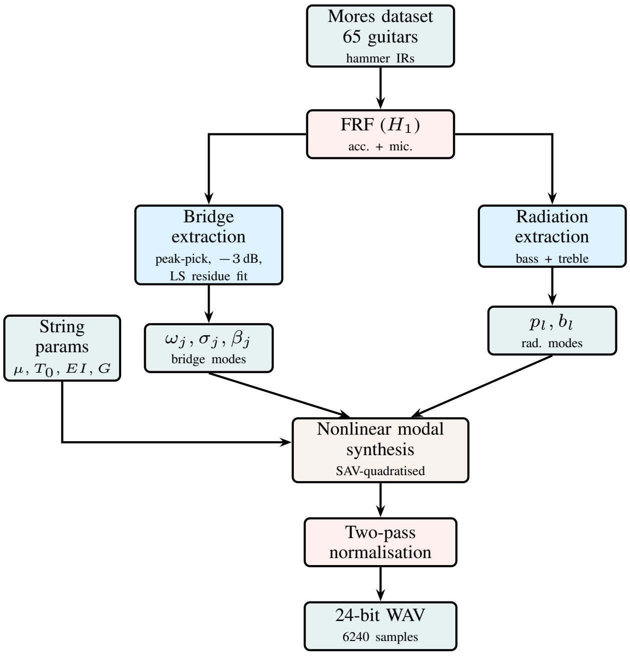

Figure 6: Processing pipeline from measurement to synthesis.

4.1. Time-Stepping Scheme

System (24), with the auxiliary variable update (21b), is advanced at rate $f_s = 1/k$, with a sampling step k, and the state $\mathbf{y}$ is approximated at time step $t = nk$, $n \in \mathbb{N}$ by the time series $\mathbf{y}^n \approx \mathbf{y}(nk)$. The forward and centred difference operators are defined, respectively, as:

$$\delta_{t+}\mathbf{u}^n = \frac{\mathbf{u}^{n+1} - \mathbf{u}^n}{k}, \quad \delta_{t\cdot}\mathbf{u}^n = \frac{\mathbf{u}^{n+1} - \mathbf{u}^{n-1}}{2k}, \tag{30}$$

and a second-order derivative approximation is obtained by composition $\delta_{tt}\mathbf{u}^n = \delta_{t+}\delta_{t-}\mathbf{u}^n$. Averaging operators are defined analogously:

$$\mu_{t+}\mathbf{u}^n = \frac{\mathbf{u}^{n+1} + \mathbf{u}^n}{2} \quad \mu_{tt}\mathbf{u}^n = \frac{\mathbf{u}^{n+1} + 2\mathbf{u}^n + \mathbf{u}^{n-1}}{4}. \tag{31}$$

These definitions extend naturally to interleaved grids: for $\psi^{n-1/2} \approx \psi((n-1/2)k)$, one has: $\delta_{t+}\psi^{n-1/2} = (\psi^{n+1/2} - \psi^{n-1/2})/k$. A scheme for system (24) reads:

$$\mathbf{T}\left(\delta_{tt}\mathbf{y}^n + \tilde{\mathbf{C}}\delta_{t\cdot}\mathbf{y}^n + \frac{1}{\mu}\mu_{t+}\psi^{n-1/2}\tilde{\boldsymbol{\eta}}^n - \mathbf{s}\, f_e^n\right) = -\tilde{\boldsymbol{\Omega}}^2\mu_{tt}\mathbf{y}^n, \tag{32a}$$

$$\delta_{t+}\psi^{n-1/2} = (\boldsymbol{\eta}^n)^\intercal\, \delta_{t\cdot}\mathbf{q}_{\mathrm{nl}}^n, \tag{32b}$$

where f_e^n is the sampled input signal, and the diagonal elements of the eigenfrequencies and damping matrices $\tilde{\boldsymbol{\Omega}}^2$ and $\tilde{\mathbf{C}}$ appear as:

$$\tilde{\omega}_m^2 = \frac{4}{k^2}\frac{1 - 2e^{-\sigma_m k}\cos\left(k\sqrt{\omega_m^2 - \sigma_m^2}\right) + e^{-2\sigma_m k}}{1 + 2e^{-\sigma_m k}\cos\left(k\sqrt{\omega_m^2 - \sigma_m^2}\right) + e^{-2\sigma_m k}}, \tag{33}$$

$$\tilde{\sigma}_m = \frac{4}{k}\frac{1 - e^{-\sigma_m k}}{1 + 2e^{-\sigma_m k}\cos\left(k\sqrt{\omega_m^2 - \sigma_m^2}\right) + e^{-2\sigma_m k}}. \tag{34}$$

This form, paired with scheme (32a), ensures that the linear part is discretised exactly [26], and it was previously employed in similar settings [7, 17]. The nonlinearity is encapsulated entirely in $\boldsymbol{\eta}^n$ and $\psi^{n-1/2}$; the latter is treated as an independent time series, and updated with the discrete chain rule (32b).

Introducing the diagonal matrix $\mathbf{D} \triangleq \mathbf{I} + \frac{k^2}{4}\tilde{\boldsymbol{\Omega}}^2 + k\tilde{\mathbf{C}}$ and expanding the operators in expression (32) yields the update:

$$\left(\mathbf{D} + \mathbf{f}\tilde{\mathbf{v}}^\intercal + \frac{k^2}{4\mu}\tilde{\mathbf{z}}^n(\tilde{\boldsymbol{\eta}}^n)^\intercal\right)\mathbf{y}^{n+1} = \mathbf{b}^n, \tag{35}$$

where it was defined $\tilde{\mathbf{v}}^\intercal \triangleq -(\mathbf{v}^\intercal\mathbf{f})^{-1}\mathbf{v}^\intercal(\mathbf{I} + \tilde{\mathbf{C}}k)$ and $\tilde{\mathbf{z}}^n \triangleq -\mathbf{f}(\mathbf{v}^\intercal\mathbf{f})^{-1}\mathbf{v}^\intercal\tilde{\boldsymbol{\eta}}^n + \tilde{\boldsymbol{\eta}}^n$. The right-hand side takes the form:

$$\mathbf{b}^n = \mathbf{b}_{\mathrm{L}}^n + \frac{k^2}{4\mu}\tilde{\mathbf{z}}^n\,(\tilde{\boldsymbol{\eta}}^n)^\intercal\,\mathbf{y}^{n-1} - \frac{k^2}{\mu}\psi^{n-1/2}\tilde{\mathbf{z}}^n, \tag{36}$$

where the linear update is

$$\mathbf{b}_{\mathrm{L}}^n = \left(2\mathbf{T} - \tfrac{k^2}{2}\tilde{\boldsymbol{\Omega}}^2\right)\mathbf{y}^n + \left(k\tilde{\mathbf{C}} - \mathbf{I} - \tfrac{k^2}{4}\tilde{\boldsymbol{\Omega}}^2 - \mathbf{f}\tilde{\mathbf{v}}^\intercal\right)\mathbf{y}^{n-1} + \mathbf{T}\mathbf{s}f_e.$$

4.2. Two Sequential Sherman–Morrison Steps

The update (35) involves two rank-one perturbations of the diagonal matrix $\mathbf{D}$: one from the bridge coupling and one from the SAV nonlinearity. Each is handled by a single application of the Sherman–Morrison (SM) formula [14], so that no matrix assembly or factorisation is required. First, define $\tilde{\mathbf{D}} \triangleq \mathbf{D} + \mathbf{f}\tilde{\mathbf{v}}^\intercal$. Then, using SM, the update in Eq. (35) is written:

$$\mathbf{y}^{n+1} = \tilde{\mathbf{D}}^{-1}\mathbf{b}^n - \frac{\frac{k^2}{4\mu}\tilde{\mathbf{D}}^{-1}\tilde{\mathbf{z}}^n\,(\tilde{\boldsymbol{\eta}}^n)^\intercal\,\tilde{\mathbf{D}}^{-1}\mathbf{b}^n}{1 + \frac{k^2}{4\mu}\,(\tilde{\boldsymbol{\eta}}^n)^\intercal\,\tilde{\mathbf{D}}^{-1}\tilde{\mathbf{z}}^n}. \tag{37}$$

The computation of the inverse $\tilde{\mathbf{D}}^{-1}$ requires a further application of SM:

$$\tilde{\mathbf{D}}^{-1} = \mathbf{D}^{-1} - \frac{\mathbf{D}^{-1}\mathbf{f}\tilde{\mathbf{v}}^\intercal\mathbf{D}^{-1}}{1 + \tilde{\mathbf{v}}^\intercal\mathbf{D}^{-1}\mathbf{f}}, \tag{38}$$

where all components can be precomputed once at initialisation. This procedure allows for keeping the total cost at $\mathcal{O}(N)$ per time step. Note that, although a unified procedure was here presented for brevity, the nonlinear update (37) is applied to the first M_{nl} modes only, while the remaining are computed as linear oscillators requiring solely the inversion (38).

4.3. Gradient computation

The entries of the SAV gradient can be computed analytically as:

$$g_i = \frac{hG}{\sqrt{2\phi_{\mathrm{nl}} + \varepsilon}}\left(\sqrt{1 + (\zeta_i)^2} - 1\right)\frac{\zeta_i}{\sqrt{1 + (\zeta_i)^2}}. \tag{39}$$

However, using the analytic expression for the SAV gradient at lower sample rates (such as audio rate) can result in anomalous behaviour of the auxiliary variable, such as sign-flip and long-term drift. The latter causes the propagated $\psi^{n-1/2}$ to drift from the analytic value $\psi_{\mathrm{true}}^n \triangleq \sqrt{2\phi_{\mathrm{nl}}(\boldsymbol{\zeta}^n) + \varepsilon}$. A servo correction, developed in [18], addresses this behaviour by adjusting the gradient along the velocity direction:

$$\bar{\mathbf{g}} = \hat{\mathbf{g}} - \frac{\psi^{n-1/2} - \psi_{\mathrm{true}}^{n-1/2}}{\|\boldsymbol{\zeta}^n - \boldsymbol{\zeta}^{n-1}\|}\left(\boldsymbol{\zeta}^n - \boldsymbol{\zeta}^{n-1}\right), \tag{40}$$

provided $\|\boldsymbol{\zeta}^n - \boldsymbol{\zeta}^{n-1}\| > 0$. Here, $\hat{\mathbf{g}}$ indicates the analytic gradient, computed with (39).

To prevent sign-flipping the constraint strategy presented in [7], consists of imposing:

$$\mu_{t+}\psi^{n-1/2} \geq 0. \tag{41}$$

This yields a scalar multiplier γ applied to the servo-corrected gradient $\bar{\mathbf{g}}$. The final gradient is set as $\mathbf{g}^n = \gamma\bar{\mathbf{g}}^n$, where

$$\gamma = \begin{cases} -\dfrac{4\psi^{n-1/2}}{\theta} & : \ \theta \neq 0 \ \& \ \theta < -4\psi^{n-1/2} \\ 1 & \text{otherwise} \end{cases} \tag{42}$$

with

$$\theta \triangleq (\boldsymbol{\eta}^n)^\intercal \left(\tilde{\mathbf{D}}^{-1}\mathbf{b}_\mathrm{L}^n - \mathbf{y}^{n-1}\right). \tag{43}$$

The regularised gradient $\mathbf{g}^n$ enters the staggered update (32b).

4.4. Bridge Force, Radiation, and Algorithm Summary

Once $\mathbf{y}^{n+1}$ is known, the bridge force can be computed explicitly with:

$$F_b^n = (\mathbf{v}^\intercal\mathbf{f})^{-1}\mathbf{v}^\intercal\left(\delta_{tt}\mathbf{y}^n + \tilde{\mathbf{C}}\delta_{t\cdot}\mathbf{y}^n + \frac{1}{\mu}\mu_{t+}\psi^{n-1/2}\tilde{\boldsymbol{\eta}}^n - \mathbf{s}f_e\right). \tag{44}$$

The resulting value drives both bass and treble radiation reverberators. Sympathetic resonance of the five unplucked strings is modelled by linear modal oscillators below a cap $f_\mathrm{symp}^\mathrm{max}$, driven by F_b with gain G_symp; the plucked-string identity is swapped from note to note, while the remaining five, driven only through bridge motion, stay well below the geometrically-exact nonlinearity threshold, justifying their linear treatment:

$$F_\mathrm{rad}^n = F_b^n + G_\mathrm{symp}\sum_l s_l^\mathrm{symp}(n). \tag{45}$$

At each time step the slope field, potential, true SAV, and gradient are evaluated; the regularisation corrections are applied; two Sherman–Morrison steps yield $\mathbf{y}^{n+1}$; ψ is updated; and the radiation filters produce the stereo output.

5. RESULTS

5.1. Extraction and Synthesis

The extraction pipeline was applied to all 65 guitars. Bridge acceleration and radiation FRFs were fitted over $[20, 10000]$ Hz and $[20, 12000]$ Hz, retaining 50–200 bridge modes and 80–300 radiation poles per side. For each guitar, plucked samples were synthesised for six strings at frets $f = 0, \ldots, 15$ ($\approx$6240 notes). String geometry follows the D'Addario EJ45 set (Table 1). Damping parameters ($T_{60,s}$, $\eta_{f,s}$) are taken from the measurements of Woodhouse [23] on D'Addario Pro Arte Composites (hard tension, 650 mm scale): $T_{60,s} \in [2.43,\ 4.58]$ s, $\eta_{f,s} \in [2.0,\ 2.5] \times 10^{-4}$ s, with the G string (string 3) being the most heavily damped of the three plain-nylon trebles, as expected from its larger diameter. Other settings are in Table 2.

Table 1: *String parameters (D'Addario EJ45). Strings 1–3: plain nylon ($\rho = 1140$ kg/m^3, $E = 2.7$ GPa); 4–6: wound ($E = 2.5$ GPa).*

s	f_0 (Hz)	d (mm)	ρ (kg/m^3)
1	329.6	0.67	1 140
2	246.9	0.82	1 140
3	196.0	1.00	1 140
4	146.8	0.79	4 500
5	110.0	0.97	5 200
6	82.4	1.15	5 900

Table 2: *Key synthesis parameters.*

Parameter	Value
Sample rate f_s	48 000 Hz
Duration	5 s
Modal freq. limit	10 000 Hz
$T_{60,s}$ at $f_{0,s}$	2.43–4.58 s
Viscous coeff. $\eta_{f,s}$	$(2.0\text{–}2.5) \times 10^{-4}$ s
Loss model	linear in ω [23]
Pluck fraction ξ_e	$[0.68, 0.82]$
Bridge position ξ_b	0.995
NL cap $f_\mathrm{nl}^\mathrm{max}$	5 000 Hz
NL stiffness scale	1.0
SAV gauge ε	10^{-16}
Symp. gain G_symp	3×10^4
Symp. cap $f_\mathrm{symp}^\mathrm{max}$	5 000 Hz

5.2. Normalisation and Computational Cost

Because bridge compliance and radiation gains vary widely across guitars, a two-pass normalisation rescales each instrument's output so that the loudest note reaches full scale, and the result is written as 24-bit WAV. In MATLAB, a single 5 s note at 48 kHz requires 0.1–0.5 s depending on the mode count; the dominant cost is the radiation filter bank. The full library of $\approx$6240 notes was generated in a few hours on a standard workstation.

6. CONCLUSIONS

A complete pipeline for the nonlinear modal synthesis of classical guitar sounds has been presented and applied to 65 instruments from the publicly available Mores dataset. Bridge compliance and radiation modal parameters are extracted from impact-response measurements and coupled to a physically motivated string model in which the geometrically exact elastic potential is reformulated via the Scalar Auxiliary Variable method at the continuous level. After discretisation, the coupled system admits a fully explicit $\mathcal{O}(N)$ update through two sequential Sherman–Morrison inversions. Exact discrete modal parameters, a nonlinear frequency cap, and a regularisation correction for the auxiliary variable ensure efficiency and robustness. The synthesised samples exhibit pitch glide, phantom partials, and instrument-specific body resonances that vary audibly across the collection. Selected sound samples, together with the synthesis code, are available at: https://github.com/Nemus-Project/65_modelled_guitars

Future directions include a real-time C++ or GPU implementation, perceptual listening tests against recordings of the same instruments, extension to coupled multi-string scenarios in which the bridge mediates energy transfer between simultaneously vibrating strings, and enrichment of the excitation model with non-plucked articulations such as fret buzz and finger slides.

7. ACKNOWLEDGMENTS

This work received funding from the European Research Council (ERC) under the European Union's Horizon 2020 research and innovation programme, Grant agreement No. 950084 NEMUS.

8. REFERENCES

[1] J.-M. Adrien, "The missing link: modal synthesis," in *Representations of Musical Signals*. Cambridge, MA: MIT Press, 1991, pp. 269–298.

[2] M. Ducceschi and C. Touzé, "Modal approach for nonlinear vibrations of damped impacted plates," *J. Sound Vib.*, vol. 383, pp. 345–363, 2016.

[3] H. A. Conklin, "Generation of partials due to nonlinear mixing in a stringed instrument," *The Journal of the Acoustical Society of America*, vol. 105, no. 1, pp. 536–545, Jan. 1999.

[4] B. Bank and L. Sujbert, "Generation of longitudinal vibrations in piano strings," *J. Acoust. Soc. Am.*, vol. 117, pp. 2268–2278, 2005.

[5] P. Morse and U. Ingard, *Theoretical acoustics*. Princeton, NJ, USA: Princeton University Press, 1968.

[6] R. Russo, S. Bilbao, and M. Ducceschi, "Scalar auxiliary variable techniques for nonlinear transverse string vibration," in *Proceedings of the IFAC Workshop on Lagrangian and Hamiltonian Methods for Non Linear Control (IFAC)*, Besançon, France, Apr. 2024, pp. 160–165.

[7] R. Russo, C. J. Webb, M. Ducceschi, and S. Bilbao, "Convergence analysis and relaxation techniques for modal scalar auxiliary variable methods applied to nonlinear transverse string vibration," *Proceedings of Meetings on Acoustics*, vol. 56, no. 1, p. 035007, 11 2025.

[8] S. Bilbao, *Numerical Sound Synthesis*. Chichester: Wiley, 2009.

[9] J. Shen, J. Xu, and J. Yang, "The scalar auxiliary variable (SAV) approach for gradient flows," *J. Comput. Phys.*, vol. 353, pp. 407–416, 2018.

[10] S. Bilbao, M. Ducceschi, and F. Zama, "Explicit exactly energy-conserving methods for Hamiltonian systems," *J. Comput. Phys.*, vol. 472, p. 111697, 2023.

[11] R. Russo, "Non-iterative numerical simulation techniques for nonlinear string vibration in musical acoustics," PhD dissertation, University of Bologna, Bologna, Italy, April 2025.

[12] M. Ducceschi and S. Bilbao, "Real-time simulation of the struck piano string with geometrically exact nonlinearity via novel quadratic Hamiltonian method," in *Proceedings of the 2020 European Nonlinear Dynamics Conference*, Lyon, France, Jul. 2022.

[13] M. Ducceschi, S. Bilbao, and C. J. Webb, "Real-time modal synthesis of nonlinearly interconnected networks," in *Proc. DAFx-23*, Copenhagen, 2023.

[14] J. Sherman and W. J. Morrison, "Adjustment of an inverse matrix corresponding to a change in one element of a given matrix," *Ann. Math. Stat.*, vol. 21, pp. 124–127, 1950.

[15] M. Ducceschi and S. Bilbao, "Non-iterative solvers for nonlinear problems: The case of collisions," in *Proceedings of the Internatinal Conference on Digital Audio Effects (DAFx)*, Birmingham, UK, Sep. 2019, pp. 17–24.

[16] G. Castera, "Modélisation, analyse numérique et simulation de la propagation des ondes longitudinales dans le piano. Application à l'étude du toucher instrumental," Ph.D. dissertation, Université de Pau et des Pays de l'Adour, Dec. 2023.

[17] M. Van Walstijn, V. Chatziioannou, and A. Bhanuprakash, "Implicit and explicit schemes for energy-stable simulation of string vibrations with collisions: refinement, analysis, and comparison," *Journal of Sound and Vibration*, vol. 569, p. 117968, Jan. 2024.

[18] T. Risse, T. Helie, and S. Bilbao, "Power-balanced drift regulation for scalar auxiliary variable methods: application to real-time simulation of nonlinear string vibrations," in *Proceedings of the International Conference on Digital Audio Effects (DAFx)*, Ancona, Italy, Sep. 2025, pp. 126–133.

[19] R. Mores, "Archive for the acoustical documentation of classical Spanish guitars, flamenco guitars and romantic guitars from private and public collections – bridge mobility," 2021. [Online]. Available: https://zenodo.org/records/4604577

[20] ——, "Sound tuning in asymmetrically braced guitars," *J. Acoust. Soc. Am.*, vol. 149, no. 2, pp. 1041–1057, 2021.

[21] M. Ducceschi, "NEMUS: Numerical restoration of historical musical instruments," ERC Project No. 950084, 2021. [Online]. Available: https://nemusproject.eu

[22] M. Ducceschi and S. Bilbao, "Linear stiff string vibrations in musical acoustics: Assessment and comparison of models," *J. Acoust. Soc. Am.*, vol. 140, no. 4, pp. 2445–2454, 2016.

[23] J. Woodhouse, "Plucked guitar transients: Comparison of measurements and synthesis," *Acta Acust. United Acust.*, vol. 90, no. 5, pp. 945–965, 2004.

[24] B. Bank, "Direct design of parallel second-order filters for instrument body modeling," in *Proc. Int. Comp. Music Conf. (ICMC)*, Copenhagen, Denmark, 2007, pp. 458–465.

[25] E. Maestre, J. S. Abel, J. O. Smith, and G. P. Scavone, "Constrained pole optimization for modal reverberation," in *Proc. 20th Int. Conf. Digital Audio Effects (DAFx-17)*, Edinburgh, UK, 2017, pp. 381–388.

[26] J. L. Cieśliński, "On the exact discretization of the classical harmonic oscillator equation," *Journal of Difference Equations and Applications*, vol. 17, no. 11, pp. 1673–1694, 2011.